Journal of Power Sources 384 (2018) 396–407

Contents lists available at ScienceDirect

Journal of Power Sources

journal homepage: www.elsevier.com/locate/jpowsour

Suitability of representative electrochemical energy storage technologies for ramp-rate control of photovoltaic power

Yu Jiang[a,*], John Fletcher[b], Patrick Burr[b], Charles Hall[a], Bowen Zheng[b], Da-Wei Wang[c], Zi Ouyang[a], Alison Lennon[a]

[a] School of Photovoltaic and Renewable Energy Engineering, UNSW Sydney, NSW 2052, Australia
[b] School of Electrical Engineering and Telecommunication, UNSW Sydney, NSW 2052, Australia
[c] Particles and Catalysis Research Group, School of Chemical Engineering, UNSW Sydney, NSW 2052, Australia

HIGHLIGHTS

- Suitability of LIBs, lead-acid batteries and ECs for ramp-rate control was studied.
- Power-normalised volume requirements show LIBs are the most suitable technology.
- LIBs with a high energy density are optimal for low ramp rates or high compliance.
- With larger PV systems, LIBs with a high power are increasingly more favourable.
- ESS with 400 Wh L^{-1} and 2300 W L^{-1} is required for 10% min^{-1} ramp rates in modules.

GRAPHICAL ABSTRACT

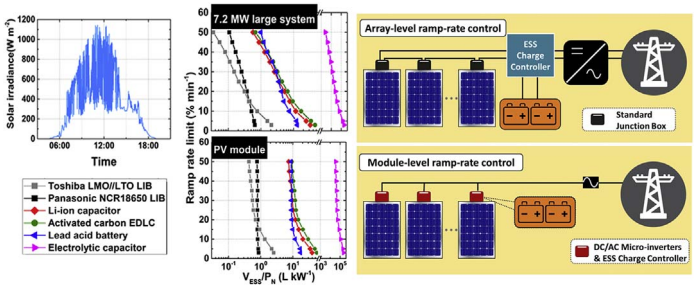

ARTICLE INFO

Keywords:
Photovoltaic
Power intermittency
Grid integration
Ramp rate control
Electrochemical energy storage technologies
Volumetric energy and power densities

ABSTRACT

Photovoltaic (PV) systems can exhibit rapid variances in their power output due to irradiance changes which can destabilise an electricity grid. This paper presents a quantitative comparison of the suitability of different electrochemical energy storage system (ESS) technologies to provide ramp-rate control of power in PV systems. Our investigations show that, for PV systems ranging from residential rooftop systems to megawatt power systems, lithium-ion batteries with high energy densities (up to 600 Wh L^{-1}) require the smallest power-normalised volumes to achieve the ramp rate limit of 10% min^{-1} with 100% compliance. As the system size increases, the ESS power-normalised volume requirements are significantly reduced due to aggregated power smoothing, with high power lithium-ion batteries becoming increasingly more favourable with increased PV system size. The possibility of module-level ramp-rate control is also introduced, and results show that achievement of a ramp rate of 10% min^{-1} with 100% compliance with typical junction box sizes will require ESS energy and power densities of 400 Wh L^{-1} and 2300 W L^{-1}, respectively. While module-level ramp-rate control can reduce the impact of solar intermittence, the requirement is challenging, especially given the need for low cost and long cycle life.

* Corresponding author. TETB Building Reception, UNSW Sydney, NSW 2052, Australia.
E-mail address: yu.jiang1@unsw.edu.au (Y. Jiang).

https://doi.org/10.1016/j.jpowsour.2018.03.013
Received 15 January 2018; Received in revised form 20 February 2018; Accepted 5 March 2018
Available online 23 March 2018
0378-7753/

1. Introduction

The world is transitioning to use more renewable energy sources, among which photovoltaics (PV) is the fastest growing accounting for almost 30% of net additions to global power capacity in 2016 [1]. However, PV systems can exhibit significant variances in their power output due to the intermittence of sunlight. As the penetration level of PV power into the utility grid continues to increase, these variances can impact voltage and frequency stability of the electricity grid, if not appropriately managed [2–5]. This is particularly problematic for small utility grids or islanded microgrids with high levels of PV penetration and limited opportunity for aggregation smoothing of the generated power [6,7].

In order to ensure the power quality and reliability of the distribution network, some utility grid operators have started to impose restrictions on the ramp rate of the generated power from grid-connected PV systems. For example, the Puerto Rico Electric Power Authority has imposed a limit of 10% of system rated capacity per minute (denoted as 10% min^{-1}) to both power ramp-up and ramp-down rates [3], and Germany requires a 10% min^{-1} limit for positive power ramps [3]. In many countries, new standards for grid connection of PV (e.g., in Australia [8]) require that inverters must implement, at least the lower level modes, demand response management modes to allow greater control over inverter response to the grid. Lower level modes require that inverters can rapidly disconnect themselves from the grid on demand, whilst higher level modes can require inverters to reduce their output to a fraction of their rated power during excursions of normal voltage and frequency operating ranges. Additional demand response management functions of ramp-rate control to allow the generated power to change smoothly from one level to another are also suggested [8,9]. Increased implementation of new grid connection standards worldwide may increase the importance of localised power-management strategies that can make possible higher penetration levels of PV in electricity grids.

PV power variability due to cloud shading can be mitigated in part by the use of module-level power-management electronics, such as DC/DC power optimisers [10,11] and DC/AC micro-inverters [2]. However, the extent of power buffering (i.e., ramp-rate control) by these electronics is inherently limited by insolation conditions. An alternative approach is to use an energy storage system (ESS) to buffer the variances by discharging to or charging from the PV generated power to compensate for PV power changes [12]. This approach enables the inverter output power to be partly decoupled from PV generated power and therefore allows more control over the power injected into the grid. Although non-electrochemical ESS technologies such as the pumped hydroelectric storage, compressed air energy storage and flywheels [2] may also be candidates for this application, this study focuses on electrochemical ESS technologies.

A range of electrochemical ESS technologies have been proposed for power buffering of PV systems [13–17]. However, most reports have assumed the use of rechargeable batteries at an array level [16,17], with some reports having also investigated the use of electrochemical double-layer capacitors (EDLCs) [14,15], or a combination of EDLCs and fuel cells [13]. Although the storage requirements (i.e., capacitance and capacity) for specific ESSs have been determined, simple justifications were made for the choices of ESS technology. Marcos et al. [18,19] and Schnabel et al. [20] derived empirical relations between the energy and power required for a generic ESS to limit the ramp rate of PV power to different levels. These studies, however, did not consider which ESS technologies would be optimal for PV power buffering applications. The energy and power density of any electrochemical ESS are correlated (with exception of the flow batteries) [21] and therefore typically need to be considered concurrently when selecting and sizing a suitable ESS.

In this paper, we incorporate into the analysis, for the first time, the volumetric energy and power densities of different electrochemical ESS technologies. Using these ESS characteristics, the suitability of a set of state-of-the-art electrochemical ESS technologies were quantitatively compared based on their required volumes for power ramp-rate control for PV systems of different sizes. Section 2 briefly reviews the ESS technologies that were considered in this study. The methods used in the study are described in Section 3 and then in Section 4 the results of the analysis are presented. First, in Section 4.1, the power generation profile for: (i) a residential rooftop PV system (5 kW); (ii) a small commercial PV power system (100 kW); and (iii) a large PV power system (7.2 MW) was simulated using 1 s solar irradiance data recorded in Sydney, Australia and a previously reported low-pass filtering method [22] to model the effects of smoothing arising from geographic aggregation and module-level electronics. A ramp-rate analysis of the solar irradiance and power generation data for a period of 46 days is presented. In Section 4.2, calculations of the power-normalised ESS volume required for different allowable ramp rate limits and compliance levels are reported, in order to determine the most suitable ESS technology for each of the different PV system sizes. Then, in Section 4.3, we introduce the new concept of PV module-level ramp-rate control, where compact ESSs are integrated into the module electronics of DC/AC micro-inverters. The requirements for an ESS for this concept and the limitations of the current ESS technologies for this application are discussed. We conclude with a discussion of the costs of the different ESS technologies and highlight the need to consider not only capital cost but also the levelised cost of storage, which takes into account the different cyclability capabilities of the different ESS technologies.

2. Electrochemical ESS technologies

The characteristics of an ESS that are of particular interest for our investigation are the energy density (storage capacity) and power density (rate capability). Although gravimetric values are commonly reported, the volume available to an ESS may be more restricted for PV ramp-rate control applications; therefore, volumetric energy and power densities are discussed in this study. Three types of ESS technologies were investigated: (i) rechargeable batteries; (ii) electrochemical capacitors; and (iii) electrolytic capacitors. Their representative energy and power densities are shown in the Ragone plot in Fig. 1.

Two examples of commonly-used rechargeable batteries that may be suitable for ramp-rate control are lithium-ion batteries (LIBs) and lead-acid batteries. Lead-acid batteries are one of the most mature and affordable ESSs and they have already been implemented in many stand-alone PV systems for load levelling [23–25]. Their energy densities are typically in the range of 50–90 Wh L^{-1} [26,27], but compared to other rechargeable batteries, their power capability is very limited. Besides, the main limitation of lead-acid batteries is their low cycle life (200–300 cycles at a 80% depth of discharge for valve-regulated lead-acid batteries [28]). Flooded lead-acid batteries have a higher cycle life but require more frequent maintenance.

Lithium-ion batteries are used commonly for portable electronic devices because of their high energy and power densities, flexibility in packaging and longer lifespan than other types of rechargeable batteries [29]. In comparison to lead-acid batteries, LIBs have substantially higher energy densities over a wide range of power densities suggesting their potential for high rate capability. State-of-the-art commercial LIBs have energy densities ranging from 200 to 700 Wh L^{-1} [30–34] and cycle lives in the order of 10^2 to 10^4 cycles [34,35]. Values vary depending on the active materials used for battery anodes and cathodes as well as device architectures. Most commercially-produced LIBs use insertion-type cathode materials, typically transition metal oxides, such as layered $LiCoO_2$ (LCO) [36], spinel $LiMn_2O_4$ (LMO) [37], layered $LiNi_{0.8}Co_{0.15}Al_{0.05}O_2$ (NCA) [38] and $LiNi_xMn_yCo_zO_2$ (NMC) with various stoichiometries [39]. Coupled with graphite anodes, commercial cells incorporating LCO or NCA cathodes can have energy densities as large as 600–700 Wh L^{-1} but a cycle life of < 1000 cycles [31,40].

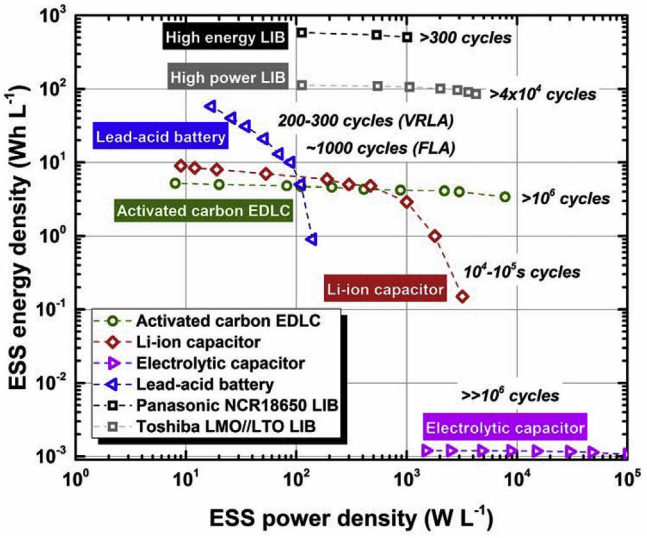

Fig. 1. Ragone plot comparing the energy and power characteristics of representative examples of different ESS technologies. For the lead-acid battery, the activated carbon EDLC, the Li-ion capacitor and the electrolytic capacitor, calculations were made based on the full device volume, including the current collectors, active material, separators, and electrolyte. Values for these devices are obtained from Ref. [61]. For the Panasonic NCR18650 [30] and Toshiba LIBs [62], volumes used in the calculations include all the aforementioned components as well as the packaging volume.

Panasonic's NCR18650 is used as an example of a high-energy LIB in Fig. 1.

Cycle life can be improved, however typically at the expense of lower energy densities, through the use of the polyanion compound $LiFePO_4$ (LFP) cathodes [41–43] (2000–3000 cycles [44]), and/or $Li_4Ti_5O_{12}$ (LTO) anodes (in the order of 10^4 cycles) [45]. Toshiba's LMO//LTO LIB is used as an example of a high-power LIB in Fig. 1. On the other hand, higher energy densities can be achieved by using conversion-type cathodes (e.g., chalcogenides (S, Se, Te) or metal halides (F^-, Cl^-, Br^-, I^-) [46,47]) or by replacing graphite with conversion-type anodes (e.g., alloy/de-alloy materials (Si, Ge, Sn) and metal oxides/phosphides/sulphides/nitrides [48]). However, conversion-type electrodes suffer from large volume changes upon lithiation and de-lithiation resulting in rapid capacity degradation with cycling [48,49]. Most conversion-type electrode materials have only been demonstrated at a research level and consequently were not considered in this study.

Electrolytic capacitors are widely used in the integrated circuit industry. They store charge electrostatically (physically) at their electrodes and can be charged very rapidly (in the order of μs to ms) and cycled many times (millions of cycles) but their energy densities (10^{-3} Wh L^{-1}) are orders of magnitude lower than rechargeable batteries [50].

Electrochemical capacitors (ECs) can provide some of the benefits of electrolytic capacitors (rapid charging/discharging and high cyclability) with increased energy densities. Current ECs can be divided into three main technology types: (i) electrochemical double-layer capacitors (EDLCs) [51–53], which store charge electrostatically through adsorption of cations and anions at the interface between the electrolyte and high surface area electrodes; (ii) pseudocapacitors [54], in which charges are additionally stored through fast reversible Faradaic reactions that occur at or near the electrode surfaces; and (iii) hybrid devices [55] comprising an EDL-type (non-Faradaic) electrode and a 'battery-type' (Faradaic) or pseudocapacitive electrode. A symmetric structure comprising two high-surface-area activated carbon electrodes is the most commercialised EDLC system. These devices have a wide operating window of power densities (typically $< 10^4$ W L^{-1} [56]) with relatively stable energy densities of < 10 Wh L^{-1} [56,57]. They can typically be cycled more than 10^6 times [50,58]. Although research level results have demonstrated that pseudocapacitive ECs can achieve higher energy densities than EDLCs, few devices been up-scaled for manufacturing. Consequently, pseudocapacitive ECs were not considered in this study.

A lithium-ion (Li-ion) capacitor is an example of hybrid ECs [59]. With appropriate device design, it has been demonstrated that higher capacitances, working voltages and therefore energy densities than a symmetric EDLC can be achieved [60]. Evident in Fig. 1, the energy densities of the Li-ion capacitor are superior to those of the activated carbon EDLC at power densities lower than ~500 W L^{-1}, but values tend to decrease rapidly at higher power densities indicating their poorer rate capability than a typical EDLC. The rate capability of the Li-ion capacitor is typically limited by the 'battery-type' electrode in which charges are stored via a slow diffusion process of lithium ions into the crystalline structure of the active material. Li-ion capacitors can have cycle lives of 10^4-10^5 cycles, lying between the LIBs and the EDLCs in the Ragone plot.

3. Methods

3.1. PV power estimation

Solar irradiance data, measured at 1 s intervals, was obtained from a rooftop weather station located at UNSW Sydney, Australia for 46 days during the period of 12 December 2015 to 23 May 2016. The weather station included a MS-402 pyranometer (EKO) and a MS-56 pyrheliometer (EKO), together with a wind speed and temperature sensor, that were configured on an automated 2-axis sun tracking system to measure the diffuse horizontal irradiance (DHI) and direct norm irradiance (DNI) respectively. The total irradiance received by a tilted PV module was computed to be the sum of the direct and diffuse components, with the direct component being calculated from the measured DNI using the method described in Ref. [63], and the diffuse component was calculated from the DHI using the method reported in Ref. [64] and a PV module tilt angle of 34°.

The PV power generation was computed from irradiance data for the different system sizes (see Table 1) using the low pass filtering method reported in Ref. [22] to simulate the smoothing provided by the geographic aggregation and the control electronics in the system. Specifically, the time series of the solar irradiance $G(t)$ (sampled with a frequency of 1 Hz) was transformed to the frequency domain ($G(s)$) using a Fast Fourier Transform and then a first-order Butterworth low-pass filter was applied to $G(s)$ according to:

$$G_f(s) = G(s)\frac{1}{(2\pi f_c)^{-1}s + 1} \quad (1)$$

where f_c denotes the cut-off frequency and s is the Laplace operator. The value of f_c, as shown in Table 1, depends on the footprint area of a PV system and was extracted from an empirical equation derived in Ref. [22]. The $G_f(s)$ signal was then transformed back to the time domain $G_f(t)$, and the power generation time series of the PV system, $P_{PV}(t)$, was calculated using:

Table 1
Characteristic of the peak power, rated power, footprint area, corresponding cut-off frequency f_c and inverse of f_c for three representative system sizes and a PV module. Values of f_c for the small and large PV power system were obtained from Ref. [22].

PV type	Peak power (kWp)	Rated power P_N (kW)	Area (Ha)	Cut-off frequency f_c (Hz)	$1/f_c$ (s)
PV module	0.28	NA	2×10^{-4}	NA	NA
Rooftop	6.7	5	0.02	0.144	6.94
Small	143	100	0.63	0.026	38
Large	9500	7243	52	0.0032	313

$$P_{PV}(t) = G_f(t) \times \frac{P_N}{G_N} \quad (2)$$

where P_N is the rated power of the PV system and G_N is the AM1.5G one-sun intensity (1000 W m^{-2}). This model was used because it was derived using actual power generation data from different sized PV systems. However, some minor inaccuracies may be present due to the different geographical location of this study (Sydney, Australia) compared to the systems used by Marcos et al. (Navarra, Spain) [22] to generate their model.

3.2. Ramp rate calculation

Maximum allowable ramp rates appeared in power system regulations are typically stated as a percentage per minute (e.g., 10% min^{-1} in Ref. [3]), however different interpretations of the ramp rate limit can lead to different estimates of ESS requirements [65]. In this study the ramp rate $r_G(t)$ was calculated for every consecutive 1 min time interval using the method stated in Ref. [18]:

$$\begin{cases} \Delta P_G(t) = \frac{\max[P_G(t-\Delta t,t)] - \min[P_G(t-\Delta t,t)]}{P_N} \\ r_G(t) = \frac{\Delta P_G(t)}{\Delta t} \end{cases} \quad (3)$$

where $P_G(t\text{-}\Delta t,t)$ is the power injected to the grid between the time $t\text{-}\Delta t$ and t, $\Delta P_G(t)$ is the power change in 1 min time period normalised to P_N, and the value of Δt is 1 min.

3.3. Ramp-rate control method

Overnight ESS charging from or discharging to the grid was assumed such that the state of charge (SoC) of the ESS was retained at zero at the beginning of each day. This way, the required ESS volume, V_{ESS}, was determined by the power output on the 'worst day' in which most irradiance fluctuation occurred. Unless otherwise mentioned, the results presented in this paper were calculated based on solar irradiance data for the 46 days for which irradiance data was available.

A schematic of the ramp-rate control method is shown in Fig. 2a. The variables, $P_{PV}(t)$, $P_G(t)$ and $P_{ESS}(t)$ are, respectively, the PV generated power, power to the grid and power to the ESSs at an instant t. Given a time series of $P_{PV}(t)$, with a sampling interval Δt (1 s measurement of data), the instantaneous ramp rate between two consecutive seconds, $r(t)$, was calculated using:

$$r(t) = \frac{P_{PV}(t) - P_G(t-\Delta t)}{\Delta t \times P_N} \quad (4)$$

In the model used, initially all the power generated by the PV system was injected into the utility grid, that is $P_G(0) = P_{PV}(0)$. Then for all $t > 0$, given a maximum allowable ramp rate limit, $r_{\max}$ (% s^{-1}), converted from $r_{\max,1min}$ (% min^{-1}), P_G at a time t was given by:

$$\begin{cases} P_G(t) = P_{PV}(t), \ \text{if } |r(t)| \le r_{\max} \\ P_G(t) = P_G(t-\Delta t) \pm r_{max} \times \Delta t \times P_N, \ \text{if } |r(t)| > r_{\max} \end{cases} \quad (5)$$

Fig. 2b depicts the P_{PV} and P_G profiles for an example 15-min time window. The difference between these two profiles is compensated by the ESSs, that is:

$$P_{ESS}(t) = P_G(t) - P_{PV}(t) \quad (6)$$

The P_{ESS} for the same time window is shown in Fig. 2c, where the shaded area indicates the energy being delivered from (positive area) or stored into (negative area) the ESSs. The ESS $SoC(t)$, shown in Fig. 2d, was calculated using [66,67]:

$$SoC_{ESS}(t) = SoC_{ESS}(0) + \int_0^t P_{ESS}(t)dt \quad (7)$$

where $SoC(0)$ is the ESS SoC in the beginning of the day (zero for the conditions used in the simulations in this study).

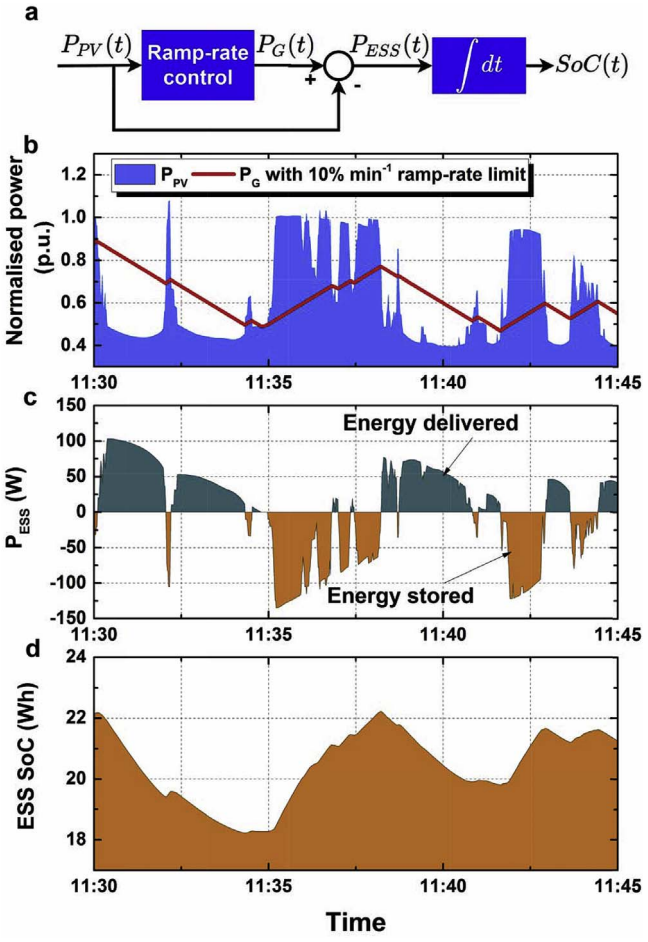

Fig. 2. a) Schematic for the ramp-rate control model that was implemented; b) normalised PV generated power without ramp-rate control and power injected into the utility grid with a ramp rate limit of 10% min^{-1}; c) power delivered from (green) or stored into (orange) ESSs during an example 15-min period; and (d) ESS SoC during the same time period. (For interpretation of the references to colour in this figure legend, the reader is referred to the Web version of this article.)

3.4. ESS volume requirements for allowable ramp rate limits

For a given $r_{\max}$, the required ESS power (in W) is the maximum absolute value of the P_{ESS} during the entire investigation period, that is:

$$P_{ESS} = \max(|P_{ESS}(0, n)|) \quad (8)$$

where 0 and n indicates the beginning and end of the time period.

The required ESS energy (in Wh) for each day was determined by:

$$E_{ESS}(d) = \max(SoC_{ESS,d}(t)) - \min(SoC_{ESS,d}(t)) \quad (9)$$

where d is the day number, and $\max(SoC_{ESS,d})$ and $\min(SoC_{ESS,d})$ are the maximum and minimum $SoC(t)$ for the day d. Then the required E_{ESS} for the entire investigation period is given by the largest value of $E_{ESS}(d)$. Since each ESS technology, can operate at a range of different energy density (E_0 to E_i) and power density (P_0 to P_i) pairs, where 0 and i indicate the endpoints of the range, the required volume V_{ESS} at each ESS operating point was determined by either the power density (e.g., P_{ESS}/P_i) or the energy density (e.g., E_{ESS}/E_i) whichever is larger. Then a series of V_{ESS} ($V_{ESS}(0)$ to $V_{ESS}(i)$) was generated and the smallest value in the series determined the minimum required V_{ESS} to meet the allowable $r_{\max}$:

$$V_{ESS} = \min\left[\max\left(\frac{P_{ESS}}{P_0}, \frac{E_{ESS}}{E_0}\right), \ldots, \max\left(\frac{P_{ESS}}{P_i}, \frac{E_{ESS}}{E_i}\right)\right] \quad (10)$$

Values of energy densities (E_0 to E_i) and power densities (P_0 to P_i) of

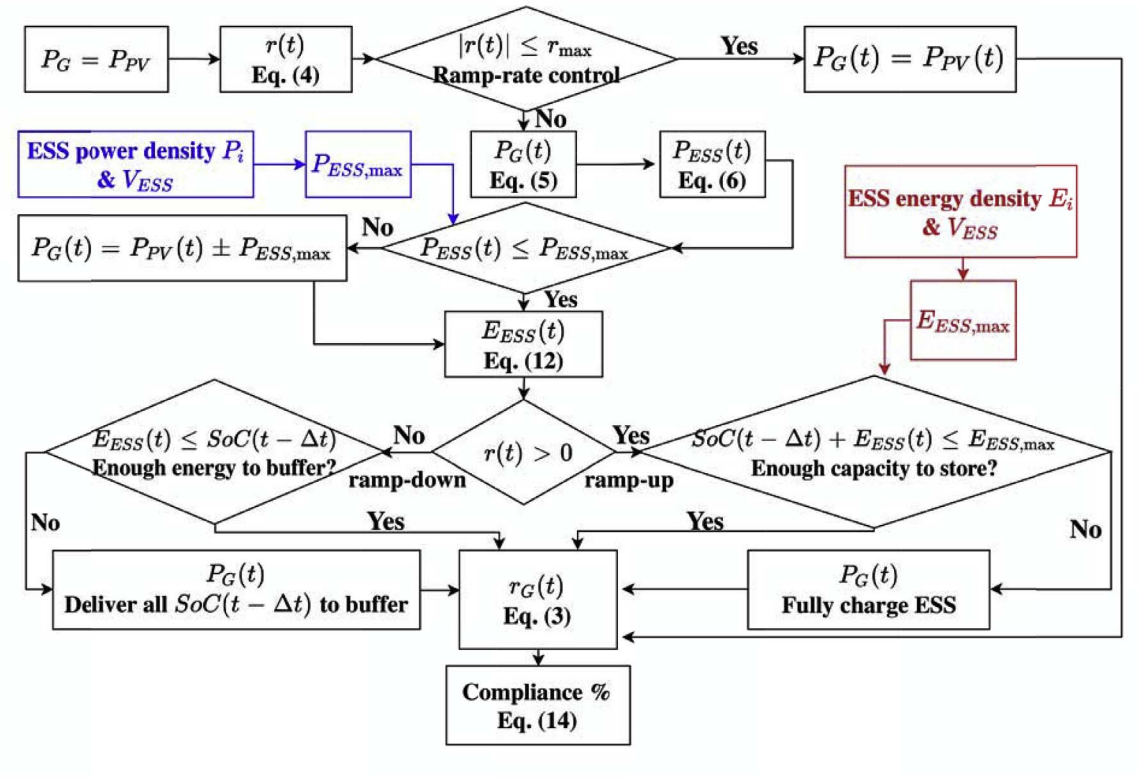

Fig. 3. Flowchart showing the computational logics used in the calculations for the achieved compliance by various ESS technologies and different V_{ESS} values.

each ESS type were obtained from Fig. 1.

3.5. Levels of compliance for selected ramp rates

Given the V_{ESS} values, the maximum energy, $E_{ESS,max}$, and power, $P_{ESS,max}$, that an ESS can provide was determined and used to calculate the levels of compliance that can be achieved for a ramp rate limit of 10% min^{-1}. A flowchart depicting the computational logic used in these calculations is shown Fig. 3. The ramp-rate control method is the same as described in Section 3.3. When $|r(t)| > r_{max}$, the ramp-rate control was activated and the compensated $P_G(t)$ was calculated using Eq. (5). The power required for this compensation, $P_{ESS}(t)$, was calculated using Eq. (6). If the ESS power was insufficient (i.e., $P_{ESS}(t) > P_{ESS,max}$), the ESS was assumed to charge or discharge at its maximum power to compensate for $P_G(t)$, that is:

$$\begin{cases} P_G(t) = P_{PV}(t) \pm P_{ESS,max}, & \text{if } P_{ESS}(t) > P_{ESS,max} \\ P_G(t) = P_G(t-\Delta t) \pm r_{max} \times \Delta t \times P_N, & \text{otherwise} \end{cases} \quad (11)$$

The energy required to provide this compensation was calculated using:

$$E_{ESS}(t) = \int_{t-\Delta t}^{t} P_{ESS}(t)dt \quad (12)$$

For ramp downs, the $SoC(t\text{-}\Delta t)$ was compared with the value of $E_{ESS}(t)$ to determine whether there was sufficient stored energy in the ESS to provide the necessary compensation. If not, the $P_G(t)$ was recalculated accordingly by assuming all $SoC(t\text{-}\Delta t)$ was delivered for buffering, that is:

$$\int_{t-\Delta t}^{t} P_{ESS}(t)dt = SoC(t-\Delta t). \quad (13)$$

For ramp ups, the algorithm was designed to examine whether there was sufficient capacity to store the $E_{ESS}(t)$, see Fig. 3. If the ESS could not accommodate all the $E_{ESS}(t)$, the excess energy was assumed to be dissipated as heat in the PV system. Using this algorithm, a time series of the compensated $P_G(t)$ was computed. The ramp rates of power injected to the grid after ramp-rate control, $r_G(t)$ (in % min^{-1}), were calculated using Eq. (3).

Finally, achieved levels of compliance at different V_{ESS} values were calculated by the ratio of the number of power ramps with rates ≤ 10% min^{-1} to the total number of power ramps:

$$\text{Compliance \%} = \frac{|\{r | r \in r_G,\ r \le r_{\max,1\,\min}\}|}{|r_G|} \times 100 \quad (14)$$

where $r_{max,1min}$ is the allowable ramp rate limit in % min^{-1} (i.e., 10% min^{-1}).

3.6. Module-level ramp-rate control

The array-level modelling described in the abovementioned sections assumes a configuration where a central ESS is placed at the DC side of the inverter to provide ramp-rate control on an array level (see Fig. 4a). In this study, we also considered the possibility where the ESS was located at the module-level (e.g., in the junction box). This scenario is depicted in Fig. 4b. Currently, more than 95% of PV modules on the market have standard junction boxes with minimal power-management electronics [68]. Adoption of 'smart' junction boxes, which incorporate advanced power-management electronics such as DC/DC power optimisers [10,11] or DC/AC micro-inverters [2], is predicted to increase to a market share of ~20% by 2027 [68]. Few reports have investigated the use of ESSs in PV systems with DC/DC power optimisers [69,70] and micro-inverters [71], and these reports have not considered the ESS requirements for this PV power buffering scenario.

We consider the specific case of an ESS being integrated into the module junction box employing a micro-inverter (shown in Fig. 4b). The modelling is also relevant to the case of DC/DC power optimisers, however in the latter case the ramp-rate control would not be integrated with DC/AC conversion. Additionally, the modelling for the

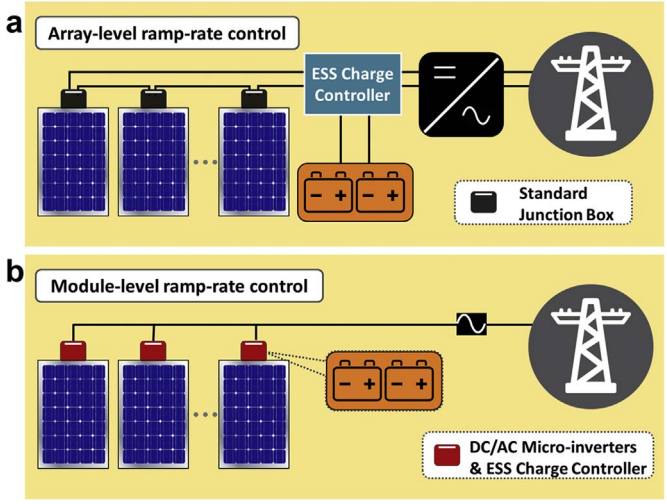

Fig. 4. Configuration of a PV system consisting of a) modules with standard junction boxes and a centralised ESS for array-level ramp-rate control; b) modules with micro-inverters and integrated-ESSs in junction boxes for module-level ramp-rate control. In b), the ESS charge controller can be also built into the module junction boxes.

DC/DC power optimiser case is made more complex due to the different architectures in which power optimisers are being implemented within modules (i.e., string-level or module-level). Module-level ramp-rate control offers several advantages over array-level control. These advantages include:

i. Increased 'plug-and-play' installation functionality;
ii. Increased system energy output by reducing the energy loss caused by the power mismatch among modules or strings;
iii. Improved system flexibility and monitoring capability;
iv. Increased redundancy to improve system reliability;
v. Integration with demand response management mode functionality in inverters (such as ramp-rate control).

However, these additional benefits are expected to be achieved at the expense of higher system costs arising from the cost of the micro-inverters and the higher ESS requirements due to limited aggregation smoothing on a module level compared to the array level. It should be noted that, in systems employing micro-inverters, implementation of an array-level ESS would require AC/DC conversion reducing the overall efficiency of the buffering functionality.

The module-level modelling assumed a PV module with peak power of 280 W [72]. The power generation of the PV module was directly computed from 1 s solar irradiance data using the normalising factor of P_N/G_N. The method used to calculate the required V_{ESS} for the various ESSs for module-level ramp-rate control was the same as described in Section 3.4. Integration of an ESS in the module junction box or power-management electronics imposes a volume restriction on the ESS. For results presented in Fig. 8, an available V_{ESS} of 0.1 L was assumed which is approximately half the volume of a current module junction box. Using this fixed V_{ESS}, the maximum energy, $E_{ESS,max}$, and power, $P_{ESS,max}$, were calculated for the selected ranges of energy and power densities. These results were then used to estimate the maximum achievable compliance to achieve a ramp rate of 10% min^{-1} at each of the energy and power density combinations using the method described in Section 3.5.

4. Results and discussion

4.1. PV power intermittency and aggregation

The 1 s solar irradiance for a typical cloudy day (13th December 2015) is shown in Fig. 5a. High-frequency fluctuations due to fast cloud passage are evident in the data. Previous reports [18,65] have noted that lower sampling frequencies can result in high-frequency

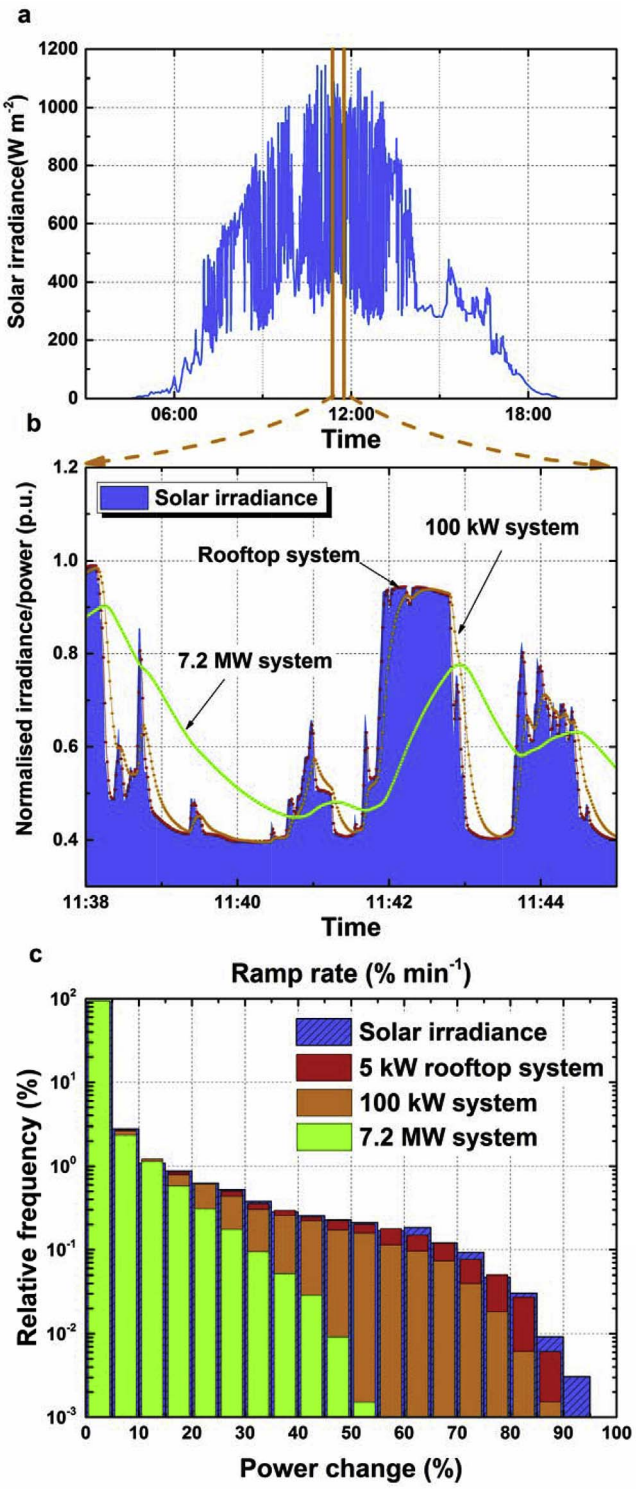

Fig. 5. a) Measured solar irradiance incident on a north-facing PV module with tilt angle of 34° in Sydney, Australia on an example cloudy day (13th December 2015). b) Measured solar irradiance and simulated power generation for a rooftop PV system, a 100 kW small PV system and a 7.2 MW large PV system between 11:38 and 11:45 a.m. The irradiance and power are normalised to the AM 1.5G one-sun intensity (1000 W m^{-2}) and the corresponding system rated power P_N, respectively. c) Frequency distributions of the ramp rates (in % min^{-1}) of solar irradiance, and power generation of a rooftop PV system, a 100 kW small PV system and a 7.2 MW large power system for an investigation period of 46 days.

fluctuations being overlooked and can therefore underestimate the PV power intermittency due to variable irradiance. Irradiance values exceeding 1000 W m^{-2}, evident around midday, can be at least partly explained by reflections of sunlight from the cloud edges [73]. A comparison of the simulated PV power generation for each of the different sized systems together with the solar irradiance data for the time period of 11:38–11:45 a.m. on the example cloudy day is shown in Fig. 5b. Instantaneous PV power and solar irradiance have been normalised by their corresponding rated power or by AM 1.5G one-sun intensity of 1000 W m^{-2}, respectively. The power output of the 5 kW rooftop PV system followed closely the profile of the irradiance due to the limited area for geographic smoothing, whilst for the small (100 kW) and large (7.2 MW) PV systems, increasing smoothing to the high-frequency fluctuations was clearly observed.

In order to quantitatively compare the smoothing achieved in each case, the changes in power and power ramp rates in a 1 min interval were calculated, and their frequency distributions are shown in Fig. 5c. The frequency histogram shows that the solar irradiance can vary as much as ~90% min^{-1} and exceeds the ramp rate limit of 10% min^{-1} for ~5% of the time (or ~ 3300 ramping incidents) during the 46 days considered in the analysis. Similar ramp rate distributions were predicted for the rooftop and small PV systems indicating that limited smoothing was occurring at a localised level. Although the high-frequency fluctuations in irradiance have been extensively smoothed by the large PV system, still ~2.4% of its power ramps (or ~ 1600 ramping incidents) exceed the limit of 10% min^{-1}. This implies that even with extensive geographic smoothing, the ramp rate of PV-generated power can exceed desirable levels for grid integration.

4.2. Array-level ramp-rate control

The 'power-normalised volume', V_{ESS}/P_N, defined as the minimum required volume for an ESS to achieve a given ramp rate limit or level of compliance divided by the rated power of the PV system, was calculated for the different ESS technologies for each of the PV system sizes. As shown in Fig. 6a, b and c, for all three PV system sizes, the required V_{ESS}/P_N is the smallest for LIBs, followed by the lead-acid battery and the ECs, and finally the electrolytic capacitor for ramp rate limits between 3% min^{-1} and 50% min^{-1}. The required V_{ESS}/P_N for all ESSs increases as the ramp rate limit becomes stricter (lower), but the increase is much greater for the ESSs with a high power density (i.e., the Toshiba high-power LIB, the Li-ion capacitor and the EDLC), than that for ESSs with a high energy density (i.e., the Panasonic high-energy LIB and the lead-acid battery). The clearly distinct slopes are due to the fact that the power requirement (P_{ESS}) determines the V_{ESS}/P_N for the energy-dense ESSs, whereas the energy requirement (E_{ESS}) determines the V_{ESS}/P_N for the power-dense ESSs. Consequently, the curves for the energy-dense ESSs and the power-dense ESS follow, respectively, the trend of the required P_{ESS} and E_{ESS} (see Fig. S1, Supporting Information). The effect of varying ramp rate limits on the E_{ESS} is more substantial, in other words, the slope of the curve is not as steep as that of the P_{ESS}. This is consistent with the observations reported by Marcos et al. [19] and Schnabel et al. [20].

For the 5 kW rooftop PV system, the smallest V_{ESS}/P_N was achieved by the Toshiba high-power LIB for ramp rate limits ≥ 20% min^{-1}. However, for ramp rate limits < 20% min^{-1}, the Panasonic high-energy LIB becomes more favourable with a V_{ESS}/P_N of ~0.8 L kW^{-1} being sufficient, compared to ~1.3 L kW^{-1} for the high-power LIB, for the limit of 10% min^{-1}. The values of V_{ESS}/P_N were calculated to be 12, 19 and 28 L kW^{-1}, respectively, for the lead-acid battery, the Li-ion capacitor and the EDLC. These are more than 10 times larger than the volume required for the LIBs. The electrolytic capacitor requires orders of magnitude larger volume compared to the other ESS technologies, and so is clearly not suitable for PV ramp-rate control on the array-level, however it was included in this comparison because it is considered below in the discussion of module-level ramp-rate control.

In the case of the 100 kW PV system, the trends are generally similar to the rooftop PV system, however the values of V_{ESS}/P_N are slightly reduced due to the geographic smoothing. For the 7.2 MW PV system, the required V_{ESS}/P_N values are substantially lower for all ESSs due to extensive geographic smoothing. The high-frequency fluctuations were eliminated, and the peak power of the PV system was reduced, leading to significantly smaller requirements for both of the E_{ESS} and P_{ESS}. The required P_{ESS} and E_{ESS} decreases with an increasing ramp rate limit at a faster rate than for the smaller PV systems (see Fig. S1, Supporting Information). This leads to the changes in the slopes of all the ESS curves (i.e., the slope is more gradual) shown in Fig. 6c. The decrease in V_{ESS}/P_N for the high-power LIB is slightly more than the high-energy LIB making the transition point between these two shifts towards lower ramp rate limit. This transition is also observed with the ECs and the lead-acid battery which implies that the high-power ESSs can be more favourable as the system size increases.

To identify the reasons behind this transition from being limited by energy density at small system sizes to being limited by power density with large PV system sizes, we compared the profile of the $P_{ESS}(t)$ and $SoC(t)$ of an ESS between the rooftop (5 kW) and the large PV system (7.2 MW) on a typical cloudy day on 13 December 2015 (see Fig. S2, Supporting Information). It was found that the required E_{ESS} reduces more than the P_{ESS} as the system size increases, indicating that the power capability of an ESS becomes more critical with increasing system size. The reduction in E_{ESS} was due to more balanced charge and discharge processes in the ESSs for the larger system. For the smaller PV systems, the high-frequency power fluctuations result in more charging or discharging events leading to significant increases in E_{ESS} requirements. Compared to the values reported by previous studies [19,20], the calculated E_{ESS} and P_{ESS} in this study are generally lower for the system with a similar size (see Fig. S1, Supporting Information). Despite of the difference in the system size, the discrepancies are at least partially due to the different geographical locations of these studies implying that the requirements for the ESSs can be sensitive to local insolation conditions.

Although meeting the ramp rate requirement at all times is ideal, practically it is more economical to select a smaller ESS volume and compromise in the level of achieved compliance. The achieved level of compliance as a function of V_{ESS}/P_N for a ramp rate limit of 10% min^{-1} is shown in Fig. 6d, e and f. At a first glance, the values of the compliance may seem acceptable (> 95%) for systems even without any ESS. However, this is due to the inclusion of the night time (i.e., when there are no power ramps) and the sunny days in the calculations for compliance.

For all three system sizes, for most compliance levels, the LIBs require the lowest V_{ESS}/P_N, followed by the ECs, the lead-acid battery and the electrolytic capacitor. More specifically, the high-power LIB required the lowest V_{ESS}/P_N for compliance lower than ~99.8% as high power densities are important to buffer the short-term fluctuations (in the order of seconds). However, for compliances higher than ~99.8%, both energy and power densities are necessary for buffering the longer fluctuations (in minutes) leading to the smallest V_{ESS}/P_N being achieved by the high-energy LIB. A similar transition in optimal ESS is also observed between the Li-ion capacitor and the EDLC, which suggests that higher power-density ESSs are more favourable for lower compliances whereas higher energy-density ESSs should be used when higher compliances are needed. Overall, the levels of compliance are higher for the larger system size due to the filtering of the short-term fluctuations by the larger system area.

We also investigated the scenario when a power curtailment of 100% P_N (i.e., 70–75% of peak power rating of PV systems) is applied to inverter output and its effects on the required V_{ESS}/P_N for an ESS. Results show that, compared to the case without power curtailment, the required V_{ESS}/P_N are generally larger. This can be attributed to the increase in the required E_{ESS} for an ESS in order to accommodate the additional proportion of PV generated power which exceeds the

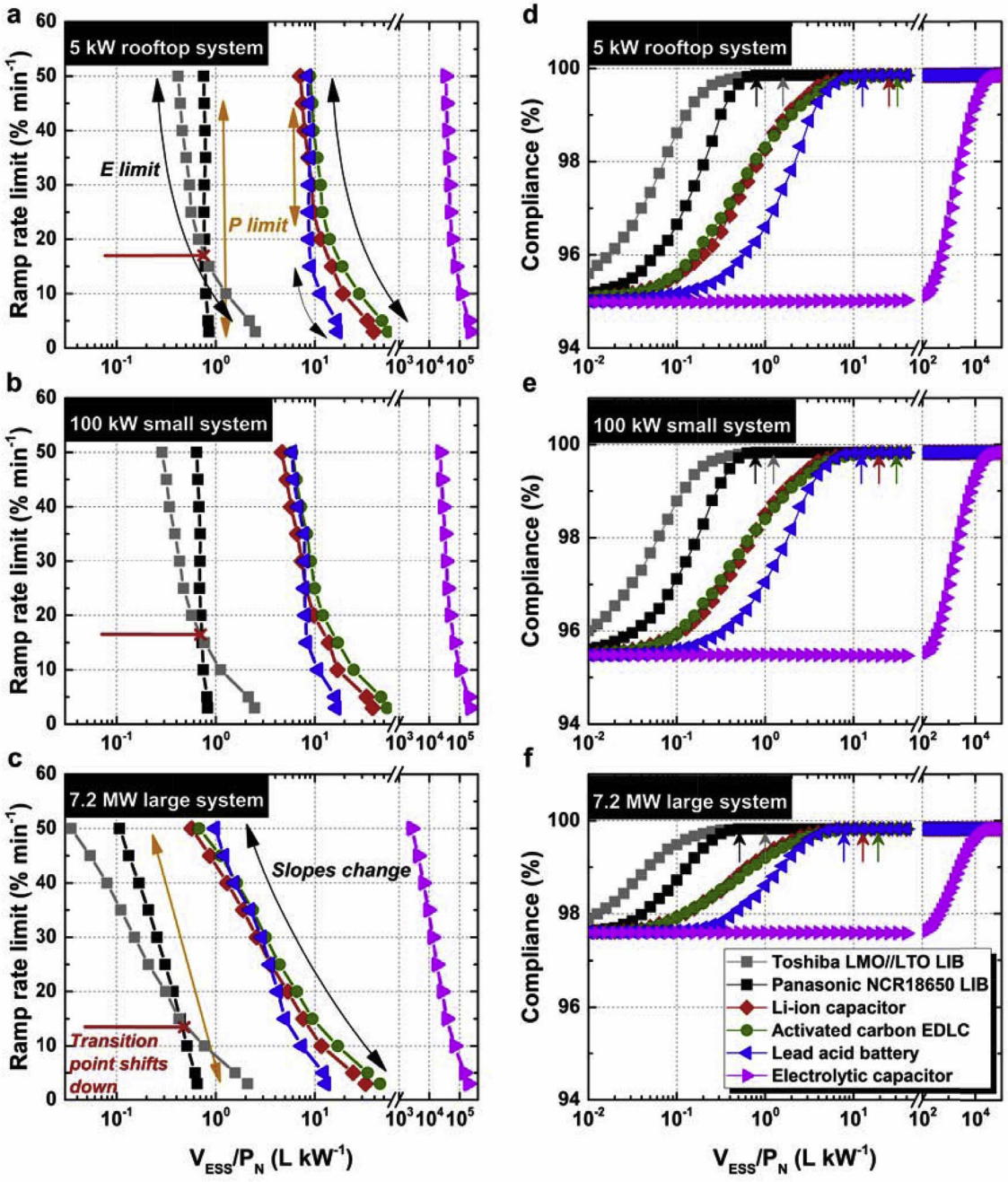

Fig. 6. Calculated ESS V_{ESS}/P_N requirements for different allowable ramp rate limits for three PV system sizes: a) a 5 kW rooftop PV system, b) a 100 kW small PV system, and c) a 7.2 MW large PV power system. The achieved levels of compliance by different ESS V_{ESS}/P_N values for three PV system sizes: d) a 5 kW rooftop PV system, e) a 100 kW small PV system, and f) a 7.2 MW large PV power system. The arrows in d), e) and f) indicate the minimum V_{ESS}/P_N values where 100% compliance has been achieved.

inverter power curtailment limit. Consequently, the rank of ESS technologies in terms of their suitability for ramp-rate control, in this scenario, is entirely dependent on their energy densities. More detailed discussion on the scenario with power curtailment can be found in Fig. S3 in Supporting Information.

4.3. Module-level ramp-rate control

Fig. 7 shows that the required values of V_{ESS}/P_N for an ESS integrated in a PV module are similar to those calculated for the 5 kW rooftop system (see Fig. 6a and d). This is not surprising as the differences between the normalised power of these two cases were minimal. For ramp rate limits ≥ 20% min^{-1} or compliance < 99.8%, the Toshiba high-power LIB was found to be the most suitable ESS. However, for a ramp rate limit of 10% min^{-1}, a smallest volume of ~0.2 L (or 0.8 L kW^{-1}) is required by the Panasonic high-energy LIB. Although this volume is sufficient to meet the energy and power requirements, the poor cycle life (> 300 cycles) of the Panasonic high-energy LIB may require the ESSs to be replaced often as buffering for short-term fluctuations in module power will require the ESSs to cycle frequently. Alternatively, the Toshiba high-power LIB with longer cycle life ($> 4 \times 10^4$ cycles) requires about twice the volume, ~0.4 L, to meet the 10% min^{-1} limit.

Current module junction boxes typically have a volume of ~0.2 L or less. Assuming half of the volume is used for connectors, diodes and other components and the other half (i.e., 0.1 L), can be used for the ESS, none of the ESS technologies considered in this study are able to meet the requirements for a ramp rate limit of 10% min^{-1}. Electrolytic

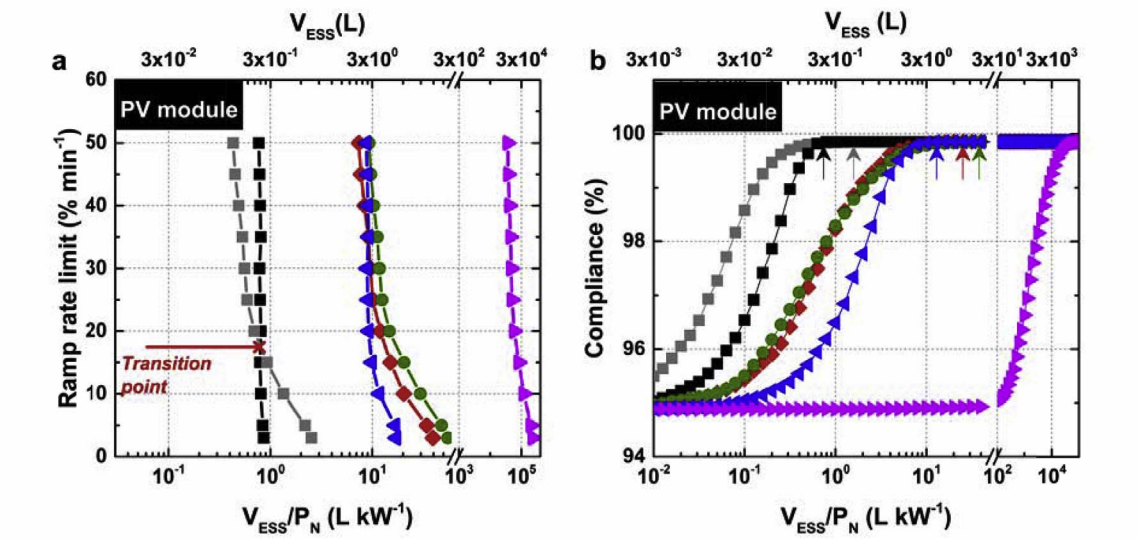

Fig. 7. Calculated V_{ESS}/P_N requirements for an integrated ESS in a PV module for: a) different allowable ramp rate limits; and b) different levels of compliance. The arrows in b) indicate the minimum V_{ESS}/P_N values where 100% compliance has been achieved.

capacitors, although perhaps a more straightforward solution as they have already been extensively used in inverter electronics, are clearly not an option for module level buffering requiring a volume in the order of 10^4 L to meet the 10% min^{-1} limit. An analysis of the required V_{ESS}/P_N when the AC power output the micro-inverters was limited to 100% of the module peak power, was also performed. The results of this analysis are presented in Fig. S4 in the Supporting Information.

Although full compliance to the grid regulations on ramp-rate control can be achieved by increasing the volumes of module junction boxes or other accessible volumes to store ESSs, some PV module technologies (e.g., bifacial PV modules) have a restricted volume that can be used for module-level electronics. This may require new approaches to junction box integration, especially if an ESS is to be incorporated at the module level.

With the restricted volume available in typical junction boxes used on current PV modules, it is useful to know which ESS technology might be most suitable for the junction box integration and the limitations. Fig. 8 shows the calculated levels of compliance obtained by different combinations of ESS energy and power densities when the ESS volume is limited to 0.1 L. The colour scales and contour lines offer a direct visualisation of the required energy and power densities to achieve a specified compliance for a 10% min^{-1} ramp rate limit, whilst the stars indicate the requirements for different ramp rate limits with 100% compliance. The energy and power characteristics of the selected ESS technologies, discussed in Section 2, are shown on the same graph. However, it should be noted that cyclability was not considered in this analysis and orders of magnitude differences in cycle life exist between the different ESS technologies that were investigated.

Both high energy and power densities are important for ESSs to achieve useful ramp-rate control at a module-level as high power densities are necessary for rapid compensation of short-term power fluctuations whilst high energy densities are required to maintain the buffering for longer periods. The energy densities of activated carbon EDLCs are still insufficient so as to limit their achievable compliance to

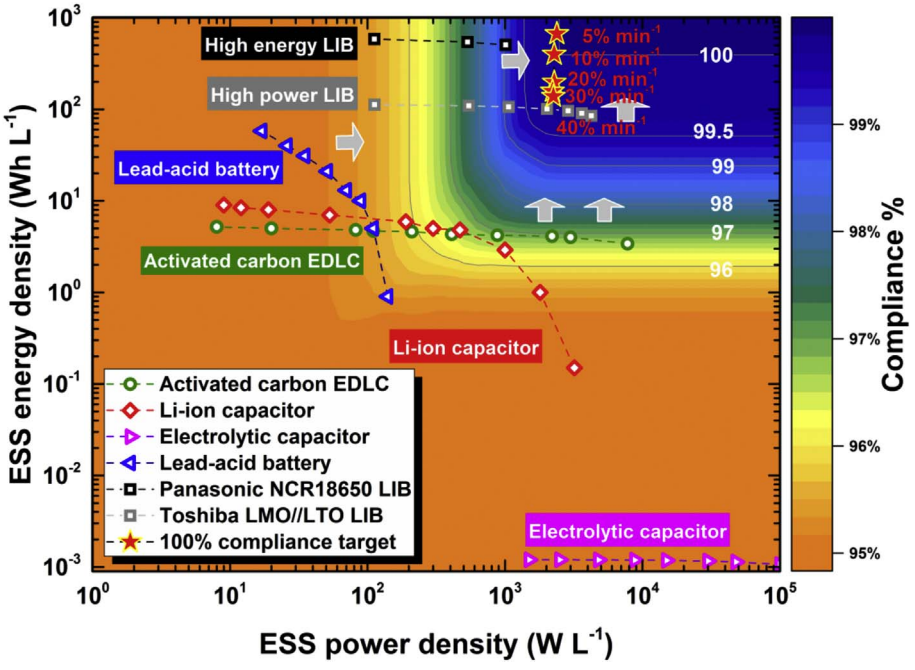

Fig. 8. Achieved levels of compliance shown as different colour scales, for a ramp rate limit of 10% min^{-1}, by different combinations of ESS energy and power densities when the ESS volume is restricted to 0.1 L. Examples of commercial-available ESS technologies are also shown on the Ragone plot. The marked stars indicate the required energy and power densities to achieve different allowable ramp rate limits with 100% compliance. (For interpretation of the references to colour in this figure legend, the reader is referred to the Web version of this article.)

~97%. Higher energy densities can be attained by the Li-ion capacitor, but the improvements only exist at lower power densities. Retaining high energy densities at fast charge/discharge power (i.e., high power densities) is crucial for Li-ion capacitors to achieve higher levels of compliance.

The ability of lead-acid batteries to reduce the power ramp rates is clearly limited by their power capability. LIBs with a high power density (e.g., the Toshiba LMO//LTO LIB) appear to be the most promising ESS technology to be used for module-level ramp-rate control. Provided that they have reasonably high energy densities as the selected Toshiba LIB example, they can achieve the ramp rate limit of 10% min^{-1} with > 99.5% compliance or almost 40% min^{-1} with 100% compliance. The power densities of the Toshiba high-power LIB are sufficient, yet further improvement in energy densities are necessary to meet the requirements for lower ramp rates or higher compliance levels. The Panasonic LIB can store > 5 times more energy than the Toshiba LIB, but its lower power densities limit its maximum achievable compliance to 99%. This implies that further increases in energy densities are unusable for this LIB without improving its power densities.

Meeting the ramp rate limit of 10% min^{-1} with 100% compliance, with the data set used, at the module level will require an ESS with a minimum energy density of ~400 Wh L^{-1} and power density of ~2300 W L^{-1}. This is a challenging design requirement that will require improved ESS materials. Not only do the materials need to provide high energy and power densities, but cost-effective ramp-rate control will require long cycling lives. It is probably not necessary for the ESS to match PV module lifetimes as junction boxes can be replaceable, and in fact there is a growing trend towards periodic replacement of junction box electronics in large PV systems as part of the maintenance cycle. This approach is consistent with aspirations to extend PV module lifetime to 30 + years as a way to reduce the levelised cost of electricity [74].

4.4. Cost of storage

For stationary applications (e.g., residential and commercial power systems), the capital cost of lead-acid batteries is in the range of US $105–635 kWh^{-1}, which is less than values of US$200–1,260 kWh^{-1} reported for LIBs [34,75]. Capital cost of lead-acid batteries and LIBs used for stationary applications was predicted to drop by about 1/2 [34] to 2/3 [76] by the year of 2030. For LIBs, the high-power LIBs utilising LTO-based materials (US$473–1260 kWh^{-1}) tend to be more expensive than the other commercial LIBs [34]. Although comparative costs and projected costs can be informative, reported estimates can vary significantly due to rapidly reducing costs occurring as a result of increases in volume manufacturing [76]. Cost comparisons between ESS technologies at different manufacturing maturity are also not necessarily meaningful.

Cost estimates need to also take into account the cost of storage and not just the capital cost. For example, for non-mature technologies such as the ECs (for which cost data are relatively scarce and variable), although the capital cost of ECs can be > 10 times that of LIBs in terms of US$ per kWh [77,78], ECs have other merits such as their low maintenance cost and long cycle lives (> 10^6 cycles) which can significantly reduce the cost of storage. Similarly, although LIBs are currently more expensive than lead-acid batteries in terms of the capital cost, their levelised cost of storage (US$891–1274 MWh^{-1}) can be comparable or even lower than that of lead-acid batteries (US $1057–1239 MWh^{-1}) [75] due to their superior electrical performance, e.g., longer cycle lives (10^2 -10^4 compared to 10^2-10^3 for the lead-acid batteries [28,34]) and higher round-trip efficiencies.

In the analysis conducted for the levelised cost of storage, an assumption of 100% depth of discharge cycle per day was used, which is a reasonable assumption for ESSs used for residential or commercial power systems for backup power storage or peak shaving [79]. However, for the PV ramp-rate control application, an ESS can be charged/discharged many times per day to buffer the short-term fluctuations and the depth of charge/discharge will vary significantly. An accurate analysis of the levelised cost of storage for this application, will therefore require not only a detailed analysis of the power generation data from PV systems (as was performed in the present paper) but also a more detailed knowledge of the charge/discharge dynamics and degradation characteristics of each ESS technology. This exercise can be challenging given the paucity of reliable and accurate data for the different ESS technologies, and in particular, less mature technologies such as ECs.

5. Conclusions and outlook

We reported a comparative evaluation of the required power-normalised volumes (V_{ESS}/P_N) for a set of representative electrochemical ESS technologies to provide power ramp-rate control for PV systems. The analysis used the volumetric energy and power densities of the different ESS technologies to determine, for three PV system sizes and a range of ramp rate limits and compliance levels, the most suitable ESS technology. For a typical residential rooftop system or a small commercial PV system, high-power LIBs require the smallest V_{ESS}/P_N for higher ramp rate limits (≥20% min^{-1}) or lower compliance (< 99.8%), whereas high-energy LIBs were predicted to be more suitable when stricter ramp rate limits or compliance are necessary. As the PV system size increases, the required V_{ESS}/P_N values are substantially lower and the power capability of an ESS becomes increasingly critical than its energy density. The large differences in the required V_{ESS}/P_N for the different ESS technologies highlight the importance of correctly selecting a suitable ESS for this application.

An alternative ramp-rate control concept of buffering at the PV module level was introduced, and the specific case of integrating an ESS with a micro-inverter located in the junction box of a PV module, was explored. It was found that the V_{ESS}/P_N requirements for this ESS configuration are similar to those for array-level ramp-rate control for the rooftop PV system, however module-level buffering offers several advantages which include: (i) 'plug-and-play' installation; ii) increased system energy output; (iii) more system flexibility and improved monitoring capability; (iv) increased redundancy to improve system reliability; and (v) inverter integration with demand response management functionality (such as ramp-rate control). The analysis concluded that LIBs are the most suitable ESS technology for this control strategy. However, when a volume restriction of 0.1 L was applied then current commercially available LIBs can only achieve a 10% min^{-1} ramp rate with ~99.5% compliance. Further reductions in ramp rates or increases in compliance require more accessible volume on the module to store ESSs, or development of ESSs with sufficient energy and power densities (a minimum of ~400 Wh L^{-1} and ~2300 W L^{-1} respectively) and long cycle lives for industrial viability.

This study demonstrates that both high energy and power density of an ESS are required for PV ramp-rate control application. Requirements for state-of-the-art ESS technologies to meet the desirable power ramp rate limits are found to be challenging, especially for buffering on a module level. Apart from advances in new ESS materials that can increase capacity and rate performance, cycle life and cost reduction, an alternative cost-competitive solution may be to design hybrid ESS forms with different technologies providing superior energy capacity and power capability respectively (e.g., LIB and EC hybrids). Then, the question lies in how to optimally configure and manage the power flow between the different ESSs. Increased use of solar forecasting and internet addressability at the site of grid integration can be used to guide this power management and make possible smarter communications between the PV systems and the utility grid in the future.

Acknowledgements

This work was supported by the Australian Research Council

through Discovery Grant DP170103219 “Advanced Electrochemical Capacitors”. The first author would like to thank the Australian Government Research Training Program for providing the PhD scholarship. The authors would like to thank Dr. Mihai Ciobotaru for providing the solar irradiance data and Dr. Ivan Perez-Wurfl for his advice with the low-pass filter.

Appendix A. Supplementary data

Supplementary data related to this article can be found at http://dx.doi.org/10.1016/j.jpowsour.2018.03.013.

References

[1] Renewables 2017: Analysis and Forecast to 2022, International Energy Agency, Paris, France, 2017.
[2] J.M. Carrasco, L.G. Franquelo, J.T. Bialasiewicz, E. Galván, R.C. Portillo Guisado, M.Á.M. Prats, J.I. León, N. Moreno-Alfonso, Power-electronic systems for the grid integration of renewable energy sources: a survey, IEEE Trans. Ind. Electron. 53 (2006) 1002–1016.
[3] V. Gevorgian, S. Booth, Review of PREPA Technical Requirements for Interconnecting Wind and Solar Generation, NREL Technical Report (2013).
[4] R. Shah, N. Mithulananthan, R.C. Bansal, V.K. Ramachandaramurthy, A review of key power system stability challenges for large-scale PV integration, Renew. Sustain. Energy Rev. 41 (2015) 1423–1436.
[5] D.M. Greenwood, K.Y. Lim, C. Patsios, P.F. Lyons, Y.S. Lim, P.C. Taylor, Frequency response services designed for energy storage, Appl. Energy 203 (2017) 115–127.
[6] X. Tan, Q. Li, H. Wang, Advances and trends of energy storage technology in Microgrid, Int. J. Electr. Power Energy Syst. 44 (2013) 179–191.
[7] G. Delille, B. Francois, G. Malarange, Dynamic frequency control support by energy storage to reduce the impact of wind and solar generation on isolated power System's inertia, IEEE Trans. Sustain. Energy 3 (2012) 931–939.
[8] AS/NZS 4777.2:2015 Grid Connection of Energy Systems via Inverters, Standards Australia, Sydney, Australia, 2015.
[9] Electric Rule 21, California Public Utilities Commission, Francisco, California, USA, (2016).
[10] S.M. MacAlpine, R.W. Erickson, M.J. Brandemuehl, Characterization of power optimizer potential to increase energy capture in photovoltaic systems operating under nonuniform conditions, IEEE Trans. Power Electron. 28 (2013) 2936–2945.
[11] A.J. Hanson, C.A. Deline, S.M. MacAlpine, J.T. Stauth, C.R. Sullivan, Partial-shading assessment of photovoltaic installations via module-level monitoring, IEEE J. Photovoltaics 4 (2014) 1618–1624.
[12] M. Beaudin, H. Zareipour, A. Schellenberglabe, W. Rosehart, Energy storage for mitigating the variability of renewable electricity sources: an updated review, Energy Sustain. Dev. 14 (2010) 302–314.
[13] T. Monai, I. Takano, H. Nishikawa, Y. Sawada, A collaborative operation method between new energy-type dispersed power supply and EDLC, IEEE Trans. Energy Convers. 19 (2004) 590–598.
[14] A. Andreotti, F. Mottola, M. Pagano, G. Velotto, Design of ultracapacitor based filter for isolated PV source feeding pulsing load, Elec. Power Syst. Res. 78 (2008) 1038–1046.
[15] N. Kakimoto, H. Satoh, S. Takayama, K. Nakamura, Ramp-rate control of photovoltaic generator with electric double-layer capacitor, IEEE Trans. Energy Convers. 24 (2009) 465–473.
[16] T.D. Hund, S. Gonzalez, K. Barrett, Grid-tied PV system energy smoothing, Photovoltaic Specialists Conference (PVSC), 2010 35th IEEE, Honolulu, HI, USA, 2010, pp. 002762–002766.
[17] X. Li, D. Hui, X. Lai, Battery energy storage station (BESS)-Based smoothing control of photovoltaic (PV) and wind power generation fluctuations, IEEE Trans Sustain. Energy 4 (2013) 464–473.
[18] J. Marcos, L. Marroyo, E. Lorenzo, D. Alvira, E. Izco, Power output fluctuations in large scale pv plants: one year observations with one second resolution and a derived analytic model, Prog. Photovoltaics Res. Appl. 19 (2011) 218–227.
[19] J. Marcos, O. Storkël, L. Marroyo, M. Garcia, E. Lorenzo, Storage requirements for PV power ramp-rate control, Sol. Energy 99 (2014) 28–35.
[20] J. Schnabel, S. Valkealahti, Energy storage requirements for PV power ramp rate control in northern europe, Int. J. Photoenergy 2016 (2016) 1–11.
[21] X. Hu, C. Zou, C. Zhang, Y. Li, Technological developments in batteries: a survey of principal roles, types, and management needs, IEEE Power Energy Mag. 15 (2017) 20–31.
[22] J. Marcos, L. Marroyo, E. Lorenzo, D. Alvira, E. Izco, From irradiance to output power fluctuations: the PV plant as a low pass filter, Prog. Photovoltaics Res. Appl. 19 (2011) 505–510.
[23] A. Hollenkamp, W. Baldsing, J. Hamilton, D. Rand, Advanced lead/acid batteries for stand-alone power-supply systems, J. Power Sources 31 (1990) 329–336.
[24] S. Hua, Q. Zhou, D. Kong, J. Ma, Application of valve-regulated lead-acid batteries for storage of solar electricity in stand-alone photovoltaic systems in the northwest areas of China, J. Power Sources 158 (2006) 1178–1185.
[25] B. Hariprakash, S. Martha, S. Ambalavanan, S. Gaffoor, A. Shukla, Comparative study of lead-acid batteries for photovoltaic stand-alone lighting systems, J. Appl. Electrochem. 38 (2008) 77–82.
[26] D. Linden, T.B. Reddy, Handbook of Batteries, McGraw-Hill, New York, 2002.
[27] S. Anuphappharadorn, S. Sukchai, C. Sirisamphanwong, N. Ketjoy, Comparison the economic analysis of the battery between lithium-ion and lead-acid in PV stand-alone application, Energy Procedia 56 (2014) 352–358.
[28] K.C. Divya, J. Østergaard, Battery energy storage technology for power systems—an overview, Elec. Power Syst. Res. 79 (2009) 511–520.
[29] J.M. Tarascon, M. Armand, Issues and challenges facing rechargeable lithium batteries, 414 (2001) 359.
[30] NCR18650 Panasonic Lithium Ion Battery, Panasonic Corporation of America, 2011, https://na.industrial.panasonic.com/products/batteries/rechargeable-batteries/lithium-ion/series/cylindrical-series/CS474 , Accessed date: 29 November 2017.
[31] M.S. Whittingham, History, evolution, and future status of energy storage, Proc. IEEE 100 (2012) 1518–1534.
[32] V. Muenzel, A.F. Hollenkamp, A.I. Bhatt, J. de Hoog, M. Brazil, D.A. Thomas, I. Mareels, A comparative testing study of commercial 18650-format lithium-ion battery cells, J. Electrochem. Soc. 162 (2015) A1592–A1600.
[33] A. Manthiram, An outlook on lithium ion battery technology, ACS Cent. Sci. 3 (2017) 1063–1069.
[34] Electricity Storage and Renewables: Cost and Markets to 2030, International Renewable Energy Agency, Abu Dhabi, UAE, 2017.
[35] A. Du Pasquier, I. Plitz, S. Menocal, G. Amatucci, A comparative study of Li-ion battery, supercapacitor and nonaqueous asymmetric hybrid devices for automotive applications, J. Power Sources 115 (2003) 171–178.
[36] K. Mizushima, P.C. Jones, P.J. Wiseman, J.B. Goodenough, LixCoO2 (0 < x < -1): a new cathode material for batteries of high energy density, Mater. Res. Bull. 15 (1980) 783–789.
[37] M.M. Thackeray, Manganese oxides for lithium batteries, Prog. Solid State Chem. 25 (1997) 1–71.
[38] C.H. Chen, J. Liu, M.E. Stoll, G. Henriksen, D.R. Vissers, K. Amine, Aluminum-doped lithium nickel cobalt oxide electrodes for high-power lithium-ion batteries, J. Power Sources 128 (2004) 278–285.
[39] N. Yabuuchi, T. Ohzuku, Novel lithium insertion material of LiCo1/3Ni1/3Mn1/3O2 for advanced lithium-ion batteries, J. Power Sources 119–121 (2003) 171–174.
[40] Panasonic NCR18650A Lithium Ion Battery, Panasonic Corporation of America, 2012, https://na.industrial.panasonic.com/sites/default/pidsa/files/panasonic-li-ion_ur18650a_datasheet.pdf , Accessed date: 29 November 2017.
[41] K.S. Nanjundaswamy, A.K. Padhi, J.B. Goodenough, S. Okada, H. Ohtsuka, H. Arai, J. Yamaki, Synthesis, redox potential evaluation and electrochemical characteristics of NASICON-related-3D framework compounds, Solid State Ionics 92 (1996) 1–10.
[42] A.K. Padhi, K.S. Nanjundaswamy, J.B. Goodenough, Phospho-olivines as positive-electrode materials for rechargeable lithium batteries, J. Electrochem. Soc. 144 (1997) 1188–1194.
[43] C. Liu, Z.G. Neale, G. Cao, Understanding electrochemical potentials of cathode materials in rechargeable batteries, Mater. Today 19 (2016) 109–123.
[44] G. Albright, J. Edie, S. Al-Hallaj, A Comparison of Lead Acid to Lithium-ion in Stationary Storage Applications, Published by AllCell Technologies LLC, 2012.
[45] K. Zaghib, M. Dontigny, A. Guerfi, P. Charest, I. Rodrigues, A. Mauger, C.M. Julien, Safe and fast-charging Li-ion battery with long shelf life for power applications, J. Power Sources 196 (2011) 3949–3954.
[46] N. Nitta, F. Wu, J.T. Lee, G. Yushin, Li-ion battery materials: present and future, Mater. Today 18 (2015) 252–264.
[47] F. Wu, G. Yushin, Conversion cathodes for rechargeable lithium and lithium-ion batteries, Energy Environ. Sci. 10 (2017) 435–459.
[48] S. Goriparti, E. Miele, F. De Angelis, E. Di Fabrizio, R. Proietti Zaccaria, C. Capiglia, Review on recent progress of nanostructured anode materials for Li-ion batteries, J. Power Sources 257 (2014) 421–443.
[49] J.-Y. Li, Q. Xu, G. Li, Y.-X. Yin, L.-J. Wan, Y.-G. Guo, Research progress regarding Si-based anode materials towards practical application in high energy density Li-ion batteries, Mater. Chem. Front. 1 (2017) 1691–1708.
[50] F. Béguin, E. Frackowiak, Supercapacitors: Materials, Systems, and Applications, Wiley-VCH Verlag GmbH, Weinheim, Germany, 2013.
[51] L. Zhang, Z. Wang, X. Hu, F. Sun, D.G. Dorrell, A comparative study of equivalent circuit models of ultracapacitors for electric vehicles, J. Power Sources 274 (2015) 899–906.
[52] M. Salanne, B. Rotenberg, K. Naoi, K. Kaneko, P.L. Taberna, C.P. Grey, B. Dunn, P. Simon, Efficient storage mechanisms for building better supercapacitors, Nature Energy 1 (2016) 16070.
[53] L. Zhang, X. Hu, Z. Wang, F. Sun, D.G. Dorrell, A review of supercapacitor modeling, estimation, and applications: a control/management perspective, Renew. Sustain. Energy Rev. 81 (2018) 1868–1878.
[54] V. Augustyn, P. Simon, B. Dunn, Pseudocapacitive oxide materials for high-rate electrochemical energy storage, Energy Environ. Sci. 7 (2014) 1597–1614.
[55] H. Wang, C. Zhu, D. Chao, Q. Yan, H.J. Fan, Nonaqueous hybrid lithium-ion and sodium-ion capacitors, Adv. Mater. 29 (2017) 1702093-n/a.
[56] A. Burke, R&D considerations for the performance and application of electrochemical capacitors, Electrochim. Acta 53 (2007) 1083–1091.
[57] Y. Gogotsi, P. Simon, True performance metrics in electrochemical energy storage, Science 334 (2011) 917–918.
[58] J.R. Miller, P. Simon, Electrochemical capacitors for energy management, Science 321 (2008) 651–652.
[59] G.G. Amatucci, F. Badway, A. Du Pasquier, T. Zheng, An asymmetric hybrid nonaqueous energy storage cell, J. Electrochem. Soc. 148 (2001) A930–A939.
[60] V. Khomenko, E. Raymundo-Piñero, F. Béguin, High-energy density graphite/AC capacitor in organic electrolyte, J. Power Sources 177 (2008) 643–651.
[61] M.F. El-Kady, M. Ihns, M. Li, J.Y. Hwang, M.F. Mousavi, L. Chaney, A.T. Lech,

R.B. Kaner, Engineering three-dimensional hybrid supercapacitors and micro-supercapacitors for high-performance integrated energy storage, Proc. Natl. Acad. Sci. U.S.A. 112 (2015) 4233–4238.
[62] A. Le Comte, Y. Reynier, C. Vincens, C. Leys, P. Azaïs, First prototypes of hybrid potassium-ion capacitor (KIC): an innovative, cost-effective energy storage technology for transportation applications, J. Power Sources 363 (2017) 34–43.
[63] A. Luque, S. Hegedus, Handbook of Photovoltaic Science and Engineering, John Wiley & Sons Ltd., Chichester, England, 2003, p. 912.
[64] Y.Q. Tian, R.J. Davies-Colley, P. Gong, B.W. Thorrold, Estimating solar radiation on slopes of arbitrary aspect, Agric. For. Meteorol. 109 (2001) 67–74.
[65] D. Cormode, A.D. Cronin, W. Richardson, A.T. Lorenzo, A.E. Brooks, D.N. Dellagiustina, Comparing ramp rates from large and small PV systems, and selection of batteries for ramp rate control, Conference Record of the IEEE Photovoltaic Specialists Conference, 2013, pp. 1805–1810.
[66] X. Wu, X. Hu, S. Moura, X. Yin, V. Pickert, Stochastic control of smart home energy management with plug-in electric vehicle battery energy storage and photovoltaic array, J. Power Sources 333 (2016) 203–212.
[67] X. Wu, X. Hu, Y. Teng, S. Qian, R. Cheng, Optimal integration of a hybrid solar-battery power source into smart home nanogrid with plug-in electric vehicle, J. Power Sources 363 (2017) 277–283.
[68] ITRPV, International Technology Roadmap for Photovoltaic 2016 Results, ITRPV, Frankfurt, Germany, 2017.
[69] Y. Du, D.D.C. Lu, Analysis of a battery-integrated boost converter for module-based series connected photovoltaic system, Power Electronics Conference IEEE, Sapporo, Japan, 2010, pp. 694–698.
[70] B.-Y. Choi, Y.-S. Noh, Y.-H. Ji, B.-K. Lee, C.-Y. Won, Battery-integrated power optimizer for PV-battery hybrid power generation system, 2012 IEEE Vehicle Power and Propulsion Conference, Seoul, South Korea, 2012, pp. 1343–1348.
[71] H. Hu, S. Harb, N. Kutkut, I. Batarseh, Z.J. Shen, A review of power decoupling techniques for microinverters with three different decoupling capacitor locations in PV systems, IEEE Trans. Power Electron. 28 (2013) 2711–2726.
[72] The Honey Framed 60-Cell Module, Trina Solar, 2017, http://static.trinasolar.com/sites/default/files/Honey%20PD05%20Australia%20Feb2017%20A.pdf , Accessed date: 30 November 2017.
[73] R. Inzunza, Y. Tawada, M. Furukawa, N. Shibata, T. Sumiya, T. Tanaka, M. Kinoshita, Behavior of a photovoltaic inverter under sudden increase in irradiance due to reflection in clouds, 2015 International Conference on Renewable Energy Research and Applications (ICRERA), Palermo, Italy, 2015, pp. 851–855.
[74] The SunShot Initiative's 2030 Goal: 3¢ per Kilowatt Hour for Solar Electricity, U.S. Department of Energy, Washington, DC, USA, 2016.
[75] LAZARD Levelized Cost of Storage Analysis - Version 3.0, LAZARD, New York, USA, 2017.
[76] O. Schmidt, A. Hawkes, A. Gambhir, I. Staffell, The future cost of electrical energy storage based on experience rates, Nature Energy 2 (2017) 17110.
[77] A. Burke, Z. Liu, H. Zhao, Present and future applications of supercapacitors in electric and hybrid vehicles, 2014 IEEE International Electric Vehicle Conference (IEVC), Florence, Italy, 2014, pp. 1–8.
[78] J.R. Miller, Applications of electrochemical capacitors, 5th International Symposium on Enhanced Electrochemical Capacitors, Jena, Germany, 2017.
[79] X. Luo, J. Wang, M. Dooner, J. Clarke, Overview of current development in electrical energy storage technologies and the application potential in power system operation, Appl. Energy 137 (2015) 511–536.